Volume 2
Number 2
April 2026
Pages 259-492

EES Solar

rsc.li/EESSolar

ISSN 3033-4063

ROYAL SOCIETY OF CHEMISTRY

PAPER

Filip Podjaski *et al.*

Sub-picosecond permittivity of carbon nitrides probed with terahertz spectroscopy: revealing high dielectric response and conductivity

EES Solar

PAPER

View Article Online
View Journal | View Issue

Cite this: *EES Sol.*, 2026, **2**, 338

Sub-picosecond permittivity of carbon nitrides probed with terahertz spectroscopy: revealing high dielectric response and conductivity

Reehab Jahangir, †[ab] Filip Podjaski, †*[ac] Paransa Alimard, [a] Sam A. J. Hillman, [a] Stuart Davidson, [b] Stefan Stoica, [b] Andreas Kafizas, [a] Mira Naftaly [b] and James R. Durrant [ac]

Received 15th October 2025
Accepted 3rd February 2026

DOI: 10.1039/d5el00170f

rsc.li/EESSolar

Organic based semiconductor materials offer emerging and sustainable solutions for solar energy conversion technologies and electronics. However, knowledge of their intrinsic (photo)physical properties is often limited, especially the effect of dielectric properties ($\varepsilon_r = \varepsilon'$) on exciton separation and charge generation at sub-picosecond timescales, which corresponds to THz frequencies. Thus, THz Time Domain Spectroscopy (THz-TDS) is used to directly and accurately extract the complex permittivity ($\boldsymbol{\varepsilon} = \varepsilon' + i\varepsilon''$) and THz conductivity ($\sigma_{THz}$) of organic Carbon Nitrides (CN_x) and other polymers and elucidate the influence of environmental humidities. Overall, the THz dielectric response ε' of CN_x surpasses other organic and even glycolated materials, and water. For the ionic and 2D carbon nitride K-PHI, complex permittivity $\boldsymbol{\varepsilon}$ was observed to be strongly humidity dependent, with both ε' and σ_{THz} doubling from dry to humid conditions (ε' from ~4 to 8, $\sigma_{THz\ 75}$ to 150 S/m, respectively). When compared to other photocatalysts, the THz dielectric response of CN_x and especially humid K-PHI is within range of well-known oxides such as TiO_2 that can efficiently generate charges from excitons, due to low exciton binding energies resulting from high ε'. The importance of dielectric property characterization on functionally relevant frequencies is thus highlighted, especially in the THz gap (0.1 – 10 THz), to understand the photophysical behaviour of organic semiconductors, even in the presence of water and hydrated ions. Such THz complex permittivity determination may also be beneficial for exploring next generation photo(electro)catalysts, electronics or ionotronics, and for computational property predictions that often require knowledge of ultrafast photophysical properties.

Broader Context

Solar energy conversion technologies are widely explored for renewable energy supply in the form of electricity and fuels, for sensors etc. Most rely on photovoltaic effects, where light absorption generates excitons that are subsequently separated into functional charges. In organic systems, this transition must overcome the exciton binding energy, which is inversely proportional to the materials' dielectric response ε_r. But its highly frequency dependent values are typically unknown in the corresponding fs-ps regime for organic semiconductors (THz gap). Hence, they are approximated from static or low frequency values, or those at much higher frequency. Using THz time domain spectroscopy, we show that the full complex permittivity, *i.e.* the dielectric response ε_r and loss factors related to THz conductivity, can be measured directly and non-invasively, on the corresponding time scales of exciton separation and charge generation. Our study focussed on various polymers and Carbon Nitrides (CN_x), and the influence of environmental effects in wetting materials. It reveals that glycolation, being used in polymers to enhance permittivity in the µs-s regime, has minor effects in the THz regime. CN_x however have unexpectedly high THz dielectric values, being larger than water. The highest values are observed for the ionic CN_x K-PHI in ambient or humid conditions, reflecting their application conditions. These are linked to synergistic ion-humidity effects, giving also rise to high THz conductivity. This highlights the crucial importance of permittivity probing in relevant conditions.

Introduction

Organic semiconductor materials are increasingly used for optoelectronic and energy conversion applications since they are often easily processable and offer bottom-up tunability for desired properties and functions.[1] A potential pathway for their exploitation in a sustainable manner, addressing increasing environmental challenges, lies in their ability to absorb visible

[a]*Department of Chemistry and Centre for Processable Electronics, Imperial College London, UK. E-mail: filip.podjaski@chem.ox.ac.uk*
[b]*National Physical Laboratory, Teddington, UK*
[c]*Department of Chemistry, University of Oxford, UK*
† equally contributed.

light and to utilise this energy for electricity generation in solar cells, as photodetectors, or for the direct photocatalytic production of fuels and chemicals. In all these processes, the absorption of photons typically generates bound excitons, that are separated into charges, driving the desired function. However, in many organic based semiconductors, such as carbon nitrides (CN_x), covalent organic frameworks, or polymer systems, light energy conversion is still less efficient than in inorganic materials or the much-studied hybrid perovskites. In particular, the generation of free charges from excitons in these materials is often a key challenge for efficient device performance.[2,3] The fundamental reason for the strong exciton recombination often observed in organic based semiconductors is linked to their relatively high exciton binding energy ΔE_{Ex_BE} (compared with inorganic semiconductors), which is related to their intrinsic real permittivity ε_r:[4]

$$\Delta E_{Ex\_BE} \approx \frac{e^2}{4\pi\varepsilon_o\varepsilon_r r} \quad (1)$$

where e is the electron charge, ε_o is vacuum permittivity, r is Coulomb radius.[5]

With low ε_r, the Coulomb attraction of excitons is poorly screened by the materials' backbones' polarizability, which affects the excitons' ability to dissociate, and thus hinders the generation, stabilization, and extraction of useful charges.[6]

The complex permittivity $\boldsymbol{\varepsilon} = \varepsilon' + i\varepsilon''$ of materials, from which static real permittivity is typically deduced in the low frequency limit (also known as dielectric constant $\varepsilon_r = \varepsilon'$; a term to be avoided nowadays), actually is a highly frequency dependent property, as depicted in Fig. 1a. Crucially, often little is known about the complex permittivity properties of materials on the relevant timescale for exciton generation and separation – this typically being in the fs-ps regime, corresponding to THz frequencies. A further challenge is that the influence of environmental factors such as water exposure on the complex permittivity of the material is typically disregarded, with exciton separation often assumed to be an intrinsic material property. This environmental factor, however, is especially relevant in wetting or porous materials that have high volume interactions with their environment, and hence also in applications such as photocatalytic water splitting.[7]

Dielectric properties are typically probed from the mHz up to the MHz regime by electrochemical impedance spectroscopy (EIS), with free space microwave dielectric measurements with Vector Network Analyzers (~0.5–300 GHz),[8–11] and by optical means (*e.g.* Spectroscopic Ellipsometry (SE)) at 10^{14}–10^{15} Hz (Peta–Hz), hence leaving out the important THz timescales, often known as the 'THz-gap' (Fig. 1a).[12–14] Water has a very high DC real permittivity ($\varepsilon'_{H_2O} \approx 74$), which has been shown to affect the intrinsic charge generation and stabilization of semiconductors.[15] However, at THz regimes, its value is very moderate ($\varepsilon'_{H_2O,\ 1.5\ THz} \approx 4.15$).[16] Both studies of the THz dielectric response of organic semiconductors, and the impact of water exposure on their response, have been very limited to date. Our study shows how to access the dielectric response of various organic semiconductors and its modification by humidity exposure, on time scales relevant for solar energy conversion and photocatalysis, by using terahertz time-domain spectroscopy (THz-TDS).

THz-TDS is an increasingly commonly available technique that allows to probe the complex permittivity $\boldsymbol{\varepsilon}$ of materials in their bulk (averaged over the volume of the probing beam interacting with the sample, no approximations required) and that have been exposed to different environments, thus providing important insights into their photophysical properties on the ps timescale and below (1 THz ~1 ps) (Fig. 1a).[17,18] For this study, different insulating polymers and the broadly employed organic semiconductor poly(3-hexylthiophene) = P3HT were chosen as references,[19] while focussing on heptazine-based CN_x materials, which are among the most widely used model organic semiconductors for various light driven energy conversion applications.[4] The materials are hence broadly studied benchmark materials, and have modifiable wetting properties that are key to probe interactions with water – while also being sufficiently processable for the characterization. CN_x are easy to synthesise and to post-functionalise, highly stable, and have visible light bandgaps (typically 2.7 to 3 eV) that are suitably positioned to drive various photo–redox reactions, such as photocatalytic water splitting. Their application areas also include environmental remediation, photodetectors and sensors, ion pumps, light driven microswimmers, photocharging and dark photocatalysis, as well as photobatteries. The latter are often linked to ionic interactions with photogenerated charges.[20]

The first THz complex permittivity measurements on these layered materials are now presented, comparing different graphitic carbon nitrides (also called gC_3N_4, which are also discussed to be the same as a 1D melon-type CN_x)[20,21] and 2D-linked poly(heptazine imide) PHI, which can contain different solvated ions in their pores (called M-PHI then), that affect their function and performance (see Fig. 1b).[22–25] The influence of exposure to humidity (water) is further studied, which commonly has a strong influence on ionic mobility, and show its potential to synergistically affect a material's real and imaginary permittivity at THz frequencies, in cases where water is strongly adsorbed.[26–30] The influence of an increase in intrinsic real permittivity and THz conductivity we describe herein is mirrored by more pronounced pre-charge signals of PHI in humid conditions, indicating modified exciton-to-charge relaxation mechanisms, measured by transient absorption spectroscopy (TAS) in the fs-ns regime, underlining the important influence of humidity on intrinsic photophysical properties. The findings are discussed in detail and especially in the context of photocatalytic reactions in water.

Results

Materials and preparation

The different CN_x were synthesized following previously reported procedures (see Experimental methods for details). Three batches of g-C_3N_4 -type CN_x were synthesised at slightly different conditions (g-C_3N_4 # 1 by annealing urea at 550 °C in air followed by an acid/base wash; g-C_3N_4 #2 by annealing urea in air at 500 °C; and g-C_3N_4 #3 by annealing urea in nitrogen at

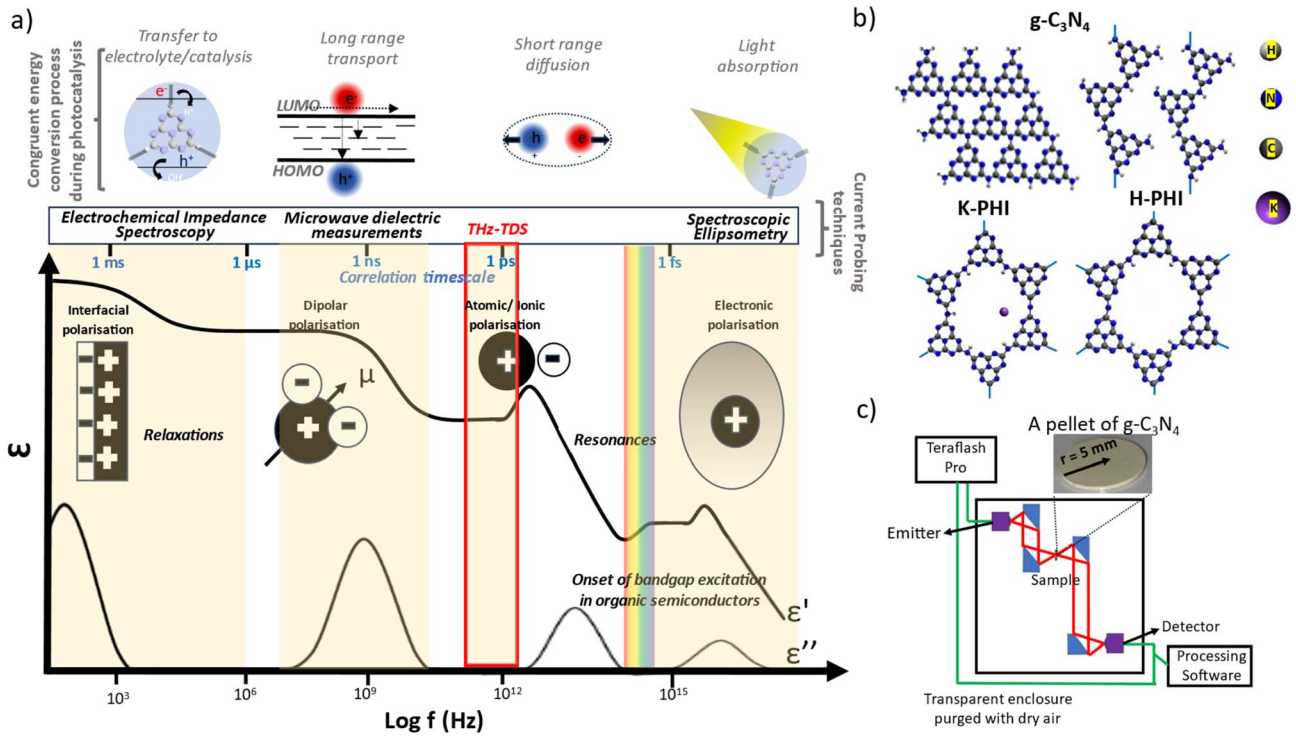

Fig. 1 Frequency-dependent complex permittivity and CN_x materials investigated. (a) Different polarisation mechanisms are activated with increasing frequency of an electric field E, leading to frequency dependent (dispersive) complex permittivity ε responses. The top scale shows the correlation of the timescale to the frequency at which these polarisation events may influence (opto)electronic properties (reproduced from [31] under the CC BY 4.0 license). (b) Schematics of atomic structures of the carbon nitrides (CN_x) investigated: the one-dimensional graphitic CN_x melon,[21] and the 2D poly(heptazine imide) PHI (here with K^+ and H^+ ions as K-PHI and H-PHI, respectively).[24] (c) Schematic of the transmission-mode Terahertz Time-Domain Spectroscopy (THz-TDS) set-up used and pictured, a processed sample of a melon pellet used for the study.

550 °C); two batches of K-PHI (derived from melamine and KSCN, K-PHI #1 by annealing g-C_3N_4 in argon at 500 °C; and K-PHI #2 by annealing g-C_3N_4 in air at 550 °C); two batches of the protonated form of PHI (H-PHI #1, #2) were obtained from the K-PHI's by acid washing.[24] Powder XRD data (Fig. S1) shows characteristic peaks at $2\Theta = 13.1°$ and 27.8° for g-C_3N_4, each corresponding to (100) and (002) the periodic arrangement of the tri-*s*-triazine rings and the interlayer stacking planes respectively,[32–34] and the prominent ~10° and ~28° peaks for K-PHI and H-PHI, corresponding to the (010) and (001) planes respectively.[25] The optical band gaps, extracted from Tauc plots and diffuse reflectance measurements, are of approx. 3 eV for the melon samples and H-PHI, and ~2.8 eV for the K-PHI samples (Fig. S2), as reported.

To study their complex permittivity by THz-TDS (see Fig. 1c), thin pellets ($d = 10$ mm) were pressed from the materials (see SI, Tables S1–S3). Since THz probes the entire sample volume, precise knowledge of porosity is required.[35] For this, the material density was measured by a He-pycnometer, resulting in 1.88(1) g cm^{-3} for melon #1 and K-PHI in ambient conditions, and 1.85(1) g cm^{-3} for H-PHI. Upon drying using conventional methods such as convection oven and desiccator, the amount of water adsorbed was reduced and stable densities of 1.72(1), 1.84(1), and 1.81(1) g cm^{-3} were obtained respectively (see Experimental Methods for more details). These were subsequently used to calculate an effective pellet porosity (see Fig. S3 and SI Note 1).

THz-TDS data was collected directly from these pellets in a custom-built chamber purged with dry compressed air to avoid the parasitic absorption of ambient water vapour (Fig. 1c). The terahertz pulse transmitted through the sample is Fourier-transformed from the time to frequency domain. The measured change in phase and amplitude relative to the reference beam allows calculation of the complex refractive index $\boldsymbol{n}$. The complex permittivity $\boldsymbol{\varepsilon}$ *is* extracted *via* $\boldsymbol{n} = \sqrt{\boldsymbol{\varepsilon}}$, including error propagation (SI Note 2). $\varepsilon'(\omega)$ depicts the frequency(ω)-dependend real permittivity (= dielectric polarisation reponse), and $\varepsilon''(\omega)$ the imaginary permittivity, which is a measure of energy dissipation due to loss mechanisms arising from polarisation, phonon contributions and accelaration of charge carriers due to the alternating electric field, relating linearly to THz conductivity (σ_{THz}, eqn S11).

Ambient measurements

First, data acquisition was veryfied on high density polyethylene (HDPE) and hygroscopic poly(ethyleneglycol) = PEG, confirming literature values and expected dispersion trends (Fig. 2 and SI Note 3). Their real permittivity at 1.5 THz is $\varepsilon'_{1.5\ THz} = 2.39$ and 2.76, respectively (Table S4). New measurements on the semiconductor P3HT show a flat dispersion profile in the range

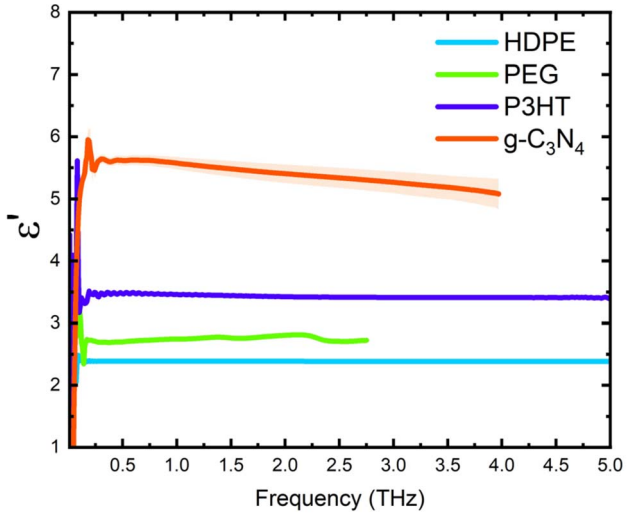

Fig. 2 Ambient real permittivity ε' for a high density poly(ethylene) = HDPE reference, poly(ethylene glycol) = PEG (M_w = 8000), and the different melon batches (as synthesised in air from urea at 550 °C (Melon # 1), at 500 °C in (Melon # 2), and at 550 °C (Melon # 3) in a custom CVD oven under nitrogen flow. See Fig. S4 for more details on ε' and THz conductivity.

probed, with $\varepsilon'_{1.5\ THz} = 3.44$. All g-$C_3N_4$ samples show very similar complex permittivity dispersion (Fig. S4, S6 and SI Note 4), with $\varepsilon'_{1.5\ THz} = 5.5$ in average being significantly higher than our reference material (+57% *vs.* P3HT, which is widely considered a the workhorse in the conjugated polymer family). This elevation in ε' could be affected by the pores of g-C_3N_4 containing trapped water molecules ($\varepsilon'_{1.5\ THz} \sim 4.15$), as these were measured in ambient conditions with 50% relative humidity (RH), which motivates further studying these materials by decoupling them from water (*vide infra*).

Overall, from Fig. 3a,d and g, one can see that the 2D PHI based materials have increased ambient real and complex permittivity values compared to 1D melon/g-C_3N_4, and that the presence of alkali metal ions in the pores (here, K^+) of PHI seems to affect the dispersion profile of the complex permittivity spectra. The average ε' of K-PHI is 6.75, which is 22% higher than the average melon value, with a less flat dispersion profile compared to all other materials. H-PHI has $\varepsilon'_{1.5\ THz} = 6.51$ (similar to K-PHI), but with 40% reduced $\varepsilon''_{1.5\ THz}$ (see Table S4 and SI Note 3).

Since the ions in PHI are not bound to the material backbone,[24,25] it appears that they are freely moving and contributing to the dielectric response, perhaps with a different (saturating) behavior than the PHI^- backbone at frequencies above 1.5 THz, giving rise to stronger levelling-off (decreasing) for these samples due to increasingly fast polarization. Although the proton mobility on H-PHI is not yet clarified, it is likely that these hydrated ions are mobile within the pore structure.[24] However, these much smaller H^+ and probably mobile ions (*via* H_3O^+) appear to result in less pronounced interactions on the THz scale (akin to water itself), which has a lower ε' than all CN_x measured herein. In the ε'' spectra, the 2D structure of PHI appears to enable a stronger response than the 1D melon, and the presence of K^+ ions seem to increase the THz response and conductivity (*vide infra*) most strongly (see SI Note 3 and 4).

Humidity dependent THz measurements

Terahertz spectroscopy is widely used to measure water contents in materials, making use of its high absorbance in the THz regime.[26–28] The complex permittivity of water is distinct and well characterised in the THz regime ($\varepsilon'_{1.5\ THz} \approx 4.1$ and $\varepsilon''_{1.5\ THz} \approx 1.9$).[16,37] While water has much higher values of ε'' than the materials in this study, its ε' is smaller than that measured for CN_x in ambient conditions, but higher than that of many common polymers like P3HT reported above. Thanks to this difference in ε' with respect to CN_x, the impact of adsorbed or structural water in these materials can also be resolved at THz frequencies. This makes THz-TDS measurements highly relevant for studying CN_x, as the practical applications of these materials typically take place in aqueous conditions. Thus, the studied materials were measured not only in their ambient state, but also when vacuum-dried and at 100% relative humidity (RH), to generate more intrinsic and application relevant insights.

As evidenced from density measurements (Fig. S3), the CN_x samples studied herein are susceptible to water uptake, with g-C_3N_4 #1 changing in density more strongly and taking longer to stabilise than K-PHI # 1 or H-PHI upon drying (ambient density: 1.88 g.cm^{-3}; dry: −8.5% for g-C_3N_4, −2.1% for K-PHI). This hydrophilic behaviour enabling water uptake is also qualitatively confirmed by contact angle measurements, with the melon samples being partially wetting (contact angles between 24° and 59°), and K-PHI & H-PHI being fully wetting (Fig. S5).

The full (dry, ambient, humid) THz-TDS datasets for g-C_3N_4, K-PHI and H-PHI are shown in Fig. 3. For g-C_3N_4 # 1 (first row, contact angle of 41°) the ε' dispersion profiles vary little as the sample is vacuum dried or exposed to 100% RH for 4 h, whereas the imaginary permittivity ε''fluctuates slightly (Fig. 2a and b respectively). Similar trends are observed for the other samples melon #2 and melon #3 (Fig. S6), which are also slightly wetting, but with different contact angles (Fig. S5a, c and d). The THz conductivity of melon changes accordingly to its ε'' (Fig. 3c), *i.e.* dropping when dried.

For K-PHI on the other hand, which is fully wetting (Fig. S5b), the water content has a strong influence on the real permittivity (Fig. 3d and Table 1), yielding an increase of more than 100% from dry ($\varepsilon'_{1.5\ THz} = 3.99$) to humid ($\varepsilon'_{1.5\ THz} = 8.24$). The behaviour of ε'' (Fig. 3e) is more complex with the ambient and wet samples showing similar ε'' above 1 THz, and hence conductivity σ_{THz}, being ∼50% higher than the dry sample. It suggests that the THz absorption and thus conductivity properties saturate with ambient water content and do not improve further. Below 1 THz, vacuum drying seems to affect the slope of ε'' – a process that is not yet understood – and potentially affected by measurement sensitivity in this range, as well as the fact that our K-PHI pellets become more fragile when dried under vacuum.

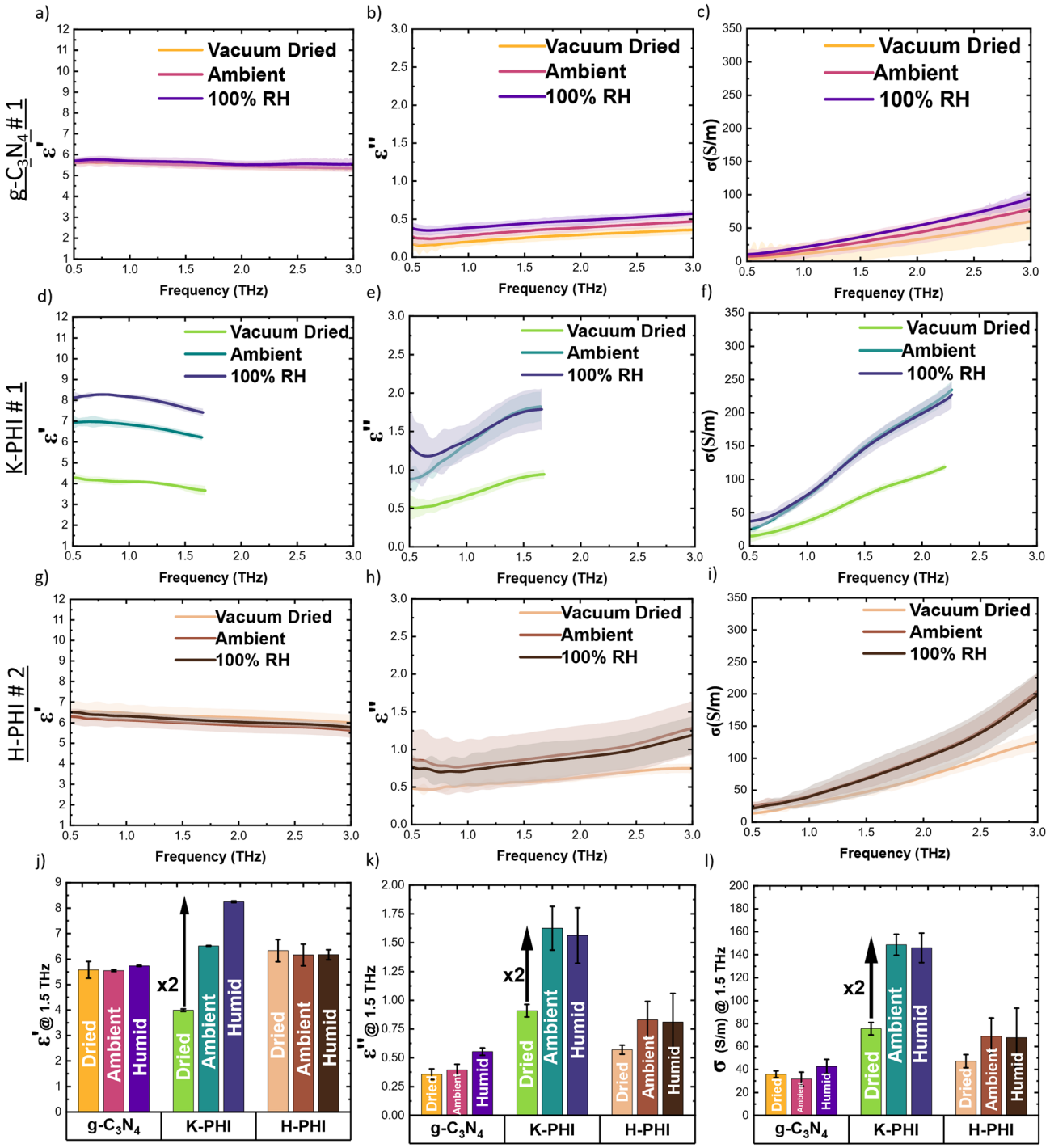

Fig. 3 Real permittivity (ε'), imaginary permittivity (ε'') and THz conductivity (σ) spectra of melon # 1 (a–c), K-PHI # 1 (d–f), H-PHI # 2 (g–i) measured in vacuum dried, ambient and 100% RH conditions, respectively. The acquired frequency range for the samples varies due to different absorption.[36] Shaded areas show the standard deviation for the respective material batch. (j–l): overview comparing the three CN_x materials at 1.5 THz across different humidity environments, error bars represent standard deviation of all respective sample types.

H-PHI shows effects in-between the other two CN_x samples. ε' is constant with respect to changes in humidity, akin to g-C_3N_4, but with a 25% higher value (Table 1), being close to ambient K-PHI (within error, Fig. 3g). ε''follows a behaviour like K-PHI, also approximately doubling upon exposure to ambient conditions, and not changing any more at 100% RH (Fig. 3h). The values for H-PHI are approximately 47% lower than for ambient K-PHI, indicating amplification effects by K^+ ions.

Fig. 3j–l summarize the humidity dependent data for ε', $\varepsilon''$and σ. Overall, the structurally porous 2D PHI materials have elevated ε' values compared to g-C_3N_4 in ambient or wet conditions, and K-PHI's ε' response significantly depends on

Table 1 Summary of complex permittivity obtained for hydrophilic materials at 1.5 THz, with red text in brackets indicating percentage change from ambient conditions. Fully wetting materials show contact angles less than 20°

	Dried		Ambient		Humid		Contact angle
Material	ε'	ε''	ε'	ε''	ε'	ε''	(°)
PEG – 8000	2.63±0.05 (-5%)	0.22±0.07 (-16%)	2.77 ± 0.01	0.19 ± 0.01	2.82±0.03 (+2%)	0.25±0.04 (+32%)	< 20
g-C_3N_4 # 1	5.46±0.02 (-0%)	0.26±0.05 (-26%)	5.60 ± 0.03	0.35 ± 0.05	5.61±0.02 (+0%)	0.44±0.03 (+26%)	41 ± 2.8
K-PHI	3.99±0.05 **(-38%)**	0.91±0.05 **(-44%)**	6.51 ± 0.01	1.62 ± 0.02	8.24±0.03 **(+27%)**	1.56±0.05 **(+0%)**	< 20
H-PHI	6.33±0.43 (-6%)	0.57±0.04 (-9%)	6.00 ± 0.42	0.86 ± 0.16	6.17±0.19 (+3%)	0.81±0.25 (-6%)	< 20

the humid environment. The ε'' of g-C_3N_4 is constantly and significantly lower than of the PHI materials. It also increases at 100% RH, which may be related to the water loss or uptake observed in density measurements (Fig. S3) and related proton mobility. Both H-PHI and K-PHI approximately double their ε'' upon exposure to ambient humidity. K-PHI shows slightly elevated values and stronger dispersion than H-PHI. σ_{THz} reflects this ε'' behaviour: g-C_3N_4 has moderate conductivity values that are slightly affected by humidity (32–40 S m^{-1} at 1.5 THz), being much lower than of the PHIs. The fact that H-PHI has elevated σ_{THz} compared to g-C_3N_4, while increasing more strongly from dry to ambient (47 to 69 S m^{-1}), points to two factors: an inherently increased ultrafast complex permittivity response with the 2D molecular backbone forming pore channels, and water playing a different, more pronounced role when adsorbed inside of PHI's confined 1D channels that do not dry out fully.[24] This is even more pronounced in K-PHI, where σ_{THz} is larger than in all humid cases of the other materials when being dry (75 S m^{-1}, >2× higher than g-C_3N_4), and doubling again in humid conditions (150 S m^{-1}), where it is > 4× higher melon and >2× than H-PHI.

Since for THz conductivity, literature values are available, where σ_{THz} was obtained directly from THz amplitude changes and using thin-film approximations, these can be put into context of other reported materials for further comparison most easily:[38] triazine based carbon nitrides, poly(triazine imide) = PTI, are structurally similar to PHI and can also contain ions in smaller pores. The ion free PTI-IF, and PTI-LiBr show σ ~7 and 35 S m^{-1} at 1.5 THz in ambient conditions, measured in free-standing pellet form.[39] The conductivity on THz timescales is hence also strongly improved by the presence of ions (*x*3.7 in PTI, compared to ~*x*2 in H– *vs.* K-PHI), albeit at lower absolute values, being only 10% for PTI-IF *vs.* H-PHI (7 *vs.* 70 S m^{-1}), and 17% in the ionic case (26 *vs.* 150 S m^{-1} for PTI-LiBr *vs.* K-PHI, albeit with different ions). A recent report on ion-free tuneable porous covalent organic framework (COF) membranes showed $\sigma_{1.5\ THz}$ between of 5.45 and 75.59 S m^{-1} for membrane samples denoted TAM-DBD and TBP-TFP respectively,[40] hence being overall in the range of CN_x, but still lower than ambient K-PHI.

These findings suggest that hydrated ion mobility contributes to much higher THz dielectric properties than expected – and that ε', ε'' and σ are hence strongly dependent on the environmental conditions the material is probed in (in dry form as neat material, or humid; more akin to application conditions). Thus it is also anticipated that processes occurring on the timescale of THz, *i.e.* the binding of excitons or charge transfer excitons, and the generation of charges, are positively influenced by the real permittivity in K-PHI in terms of solar energy conversion applications, and especially those in the presence of humidity and water. We hence investigated these materials using fs-ns TAS.

fs-ps transient absorption spectroscopy (TAS) measurements

The real THz permittivity, which corresponds to the picosecond timescale, is an important factor for the Coulomb binding of excitons and the generation of charges by exciton or charge transfer exciton dissociation and their relaxation (eqn (1)). To provide further evidence of the influence of humidity on the dissociation of (bound) excitons to free charges, the charge carrier generation properties of K-PHI samples in ambient and humid conditions were studied using fs-ns TAS. The results are shown in Fig. S8. Panels a) and b) show the spectra of a vacuum-dried K-PHI film in ambient and humid conditions from 0.2 ps to 5 ns, with the signal normalized at each delay time to illustrate temporal shape changes (see Fig. S9 a and c for raw data). After excitation with 355 nm light pulses, the material has a pronounced broad absorption signal which appears to red shift from 600 to 670 nm over 5 ns. The latter-timescale 670 nm feature is assigned to electron absorbance in the K-PHI following bandgap excitation.[41–45] From normalized data at each time snapshot, it can be observed that this red-shift begins within the first ps, and hence has a 2nd contribution before stable charge formation. The shape of the 500–650 nm shoulder is much more pronounced in humid conditions than in dry conditions (Fig. S8 b *vs.* a), clearly indicating the impact of

humidity on ultrafast dynamics of K-PHI. Using global analysis, or simple subtraction of early (sub-ps) and late (ns) signals, the spectra can be deconvoluted into two distinct parts (Fig. S8c), with the red part displaying the shoulder component. This allows to compare the relative amplitude and decay (Fig S9–S11) for ambient and humid conditions, respectively. It is possible that the shoulder in the 500–650 nm region is linked to an excitonic or exciton-related state.[44] Since the true nature cannot be clarified yet, it is termed as unrelaxed (pre-charge) signal. This signal peaks at times <1 ps and decays while the charge signal rises (peaking at 30–50 ps), consistent with a typical (charge transfer) exciton dissociation into charges, or simply charge related relaxation process (see Fig S10 and S11 for fluence dependent data). It is found that this unrelaxed signal is consistently more pronounced in the wet samples comparted to the ambient ones (~+20%, Fig. S9e). This observation hence suggests that the more pronounced, unrelaxed pre-charge feature existing on the sub-ps timescale is a consequence of water-induced backbone polarization increasing the dielectric screening and hence impacting the photophysics and decay of excited states. Although the details of spectral assignment for the nature of such excitonic/unrelaxed states requires further dedicated efforts, this measurement underlines an important role of humidity for modifying the K-PHI real permittivity response to photoexcitation in the 0.5 to 5 ns regime, corresponding to the THz frequency range probed. This analysis also directly shows that the yield of this ps-signal can be modified in the material by the presence of water, which is linked to increasing real permittivity in K-PHI, enabling the stabilization of light-induced species that subsequently relax into charges.

Discussion

Using THz-TDS, it is shown that the g-C_3N_4 and PHIs have a relatively high complex permittivity in the THz regime compared with HDPE, PEG and P3HT, qualifying CN_x as High Refractive Index Polymers (HRIP), a class of materials that could be useful for many advanced flexible optoelectronic applications such as anti-reflective coatings and encapsulants for OLEDs,[46] along with photovoltaic and photocatalytic applications. The real permittivity of proton-terminated g-C_3N_4 and H-PHI does not vary much with humidity. As a result, it can be concluded that water cannot fully account for the relatively higher complex permittivity values we see in g-C_3N_4 but is rather a result of its unique chemical structure when compared to P3HT. The heteroaromatic rings with the –C=N–C– bonds forming an extended conjugated network likely contribute to the molecular polarizability α of g-C_3N_4, thus elevating its real permittivity ε' (described by the Clausius Mossoti relation (eqn (2))) beyond that of a conjugated polymer such as P3HT:[47]

$$\frac{\varepsilon' - 1}{\varepsilon' + 2} = \frac{N\alpha}{3\varepsilon_o} \quad (2)$$

where N is the number density of the molecules (m^{-3}), and α is the molecular polarizability ($Cm^2\ V^{-1}$).

Free water ($\varepsilon'_{1.5\ THZ}$ ~4.15), which may be the reason for slight changes in ε' in presence of humidity (see Table 1, PEG *e.g.*), can also be ruled out from K-PHI's increased permittivity, since the measured ε spectra cannot be explained by a linear contribution of water adding to complex permittivity (see SI Note 5 and Fig. S11).

So far, it can also be summarized that K-PHI in a dry, intrinsic state has a lower real THz-permittivity than g-C_3N_4, but with the ions present in the 2D structure and responding to water, ε' can be doubled, far beyond g-C_3N_4, H-PHI and water alone (Fig. 2i).

ε'_{THz} in context to other materials

Fig. 4 shows the real permittivity of typical inorganic semiconductors used for solar energy conversion and compares them with organic materials and this study. Indeed, it is found that slightly elevated values exist for solar cell materials like Si or GaAs ($\varepsilon'_{1.5THz}$ >10), but many others show only modest values being in the range of humidity variations of K-PHI, *i.e.* $\varepsilon'_{1.5THz}$ = 3–8: *e.g.* the hybrid perovskite $CH_3NH_3PbI_3$, II–VI semiconductors like CdTe, and oxide semiconductors like TiO_2 or Fe_2O_3 used frequently for photo(electro)catalysis. The often-made generalization that inorganic materials have higher dielectric response than organic materials, enabling better exciton separation,[4] may therefore not be universally true in the THz regime. It can also be noted that exchange of the mobile A-site cation in the lead halide perovskites from methylammonium (CH_3NH_3) to Cs also show drastic changes in THz permittivity ($\varepsilon'_{1.5THz}$ changes from ~7.7 (ref. 4) (ref. 48) to ~20.5 (ref. 4) (ref. 49)) despite only a fraction (cation) of the material being modified.

Influence of structure and ions

In K-PHI, pore ions (K^+) are in a hydrated state and loosely bound to the 2D PHI^- backbone.[24,25] It is therefore suggested

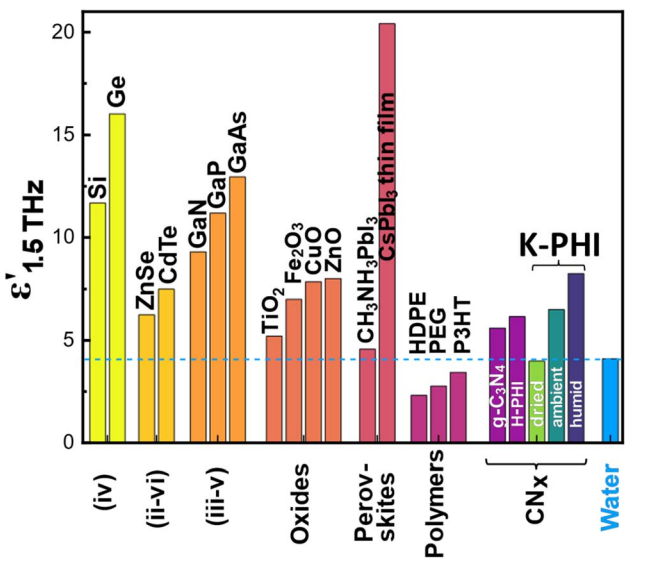

Fig. 4 Real permittivity at 1.5 THz ($\varepsilon'_{1.5THz}$) for common semiconductor materials used for solar energy conversion applications, relative to measured CN_x and water.[48–58]

that these ions, confined in 1D pore PHI channels, have an important impact on the photophysics of K-PHI in the THz regime. A closer look shows K-PHI's ambient and humid ε' profile rises slightly initially and drops beyond 0.75 THz (Fig. 3d). This indicates that the lower frequency range (0.25–0.75 THz) might capture a snapshot of the ionic (pore confined, hydrated K^+) polarisation contributing initially, and then becoming less active as the K^+ ions become unable to respond to the alternating electric field above 1 THz (maximum response time is exceeded). H-PHI on the other hand maintains a relatively constant dispersion profile across the frequency spectrum, possibly due to the much lighter H^+ ions having a more constant response across the frequencies probed (Fig. 3g). The monotonous dispersion trend in H-PHI and its ε' values close to K-PHI in ambient conditions suggest that the dominant differences between 1D g-C_3N_4 and 2D PHI arises from the covalent 2D structure with 1D pore channels in PHI itself, and by the presence of water affecting hydrated ion motion (of H^+ and K^+) on THz timescales therein. In particular, K-PHI's significantly larger ε' in humid or aqueous conditions (+100% *vs.* dry) should in theory faciliate the separation of excitons and charges through decreased Coulomb attraction, whilst more agile polarization should increase charge generation and transport on a fs-ps-timescale. The TAS data in this study provides preliminary evidence for this, with additional (probably excitonic) signals on the timescale between 0.2 and 100 ps arising more pronouncedly in conditions with higher permittivity.

Relation to complex permittivity and conductivity

Upon drying, a decrease in ε' is observed in K-PHI, likely related to lower hydrated K^+ ion motion due to a reduction in the water content within the 1D pore channel. However, some water is still expected to be trapped in the pores.[24,25] In H-PHI, the residual water may still contribute sufficiently to polarization inducing proton mobility, and thus explain the unchanged ε' values upon vacuum drying. This can be further rationalized when discussing conductivity, σ_{THz} (being linearly related to ε'', eqn S11): an earlier report on the dominantly ionic conductivity of metal-containing PHI (M-PHI) with different ions, including EIS and NMR probing ionic mobilities on different length scales, indicated that the ionic mobility of M-PHI, contributing to the conductivity in the probed 10^{-3}-10^{6} Hz range, drops significantly when the samples are dried – as in the THz case. On the other hand, the enhancement effect of hydrated ion motion showed an onset of saturation at ambient RH values. This is consistent with the findings in this study, which now extend the frequency regime to the THz timescale: the value of $\varepsilon''_{1.5\ THz}$ the σ_{THz} are similar for both ambient and 100% RH conditions for each, H– and K-PHI respectively, and halve in dry conditions. Akin to EIS measurements, the influence of adsorbed structural water on material properties saturates in ambient conditions, and the conductivity effects are stronger with metallic ions. In the EIS regime, H-PHI has conductivities order of magnitude below K-PHI – probably since aqueous protons do not have dominant effects in this mHz–MHz frequency range. In the THz regime, H-PHI shows comparably high conductivity values, but K-PHI has $\sigma_{1.5\ THz}$ 67% higher than H-PHI (see Fig. S4), indicating that the larger and heavier K^+ ions experience stronger acceleration and resistance within the THz alternating electric field, leading to stronger wave dissipation – but that protons also respond similarly in the 2D H-PHI network on fs-ps timescales.

The high ε' values of humid K-PHI cannot be explained solely by the presence of water in isolation. The humidity data in this study instead suggests that water affects the ε' of K-PHI through synergistic interactions with ions – likely caused inside structural pore channels. It is suggested that this synergy may occur also in other porous, hydrophilic materials. Such an enhancement in ε'_{THz} (for exciton separation and for charge accumulation inside the material) and in ε''_{THz} (resulting in good conductivity effects on ultrafast fs-ps timescales) seems a key and highly desirable feature for efficient direct conversion of solar energy to fuels in presence of water, as aqueous conditions can apparently boost ε' responsible for exciton dissociation and charge accumulation in the inner volume of the material, on timescales at which these processes occur. At the same timescale, when charges are just formed, boosted σ_{THz} improves charge transport and hence their extraction. These findings are likely a key factor for the enhanced activity for photocatalytic hydrogen evolution reported for PHI-materials compared to g-C_3N_4,[24,59] although the overall photocatalytic process is more complex and contains also other factors that need to be considered for efficiencies.[60]

Context to other real permittivity techniques

As explained in the introduction, the dielectric properties of materials are strongly dispersive across the frequency range from 1 Hz up to $\sim 10^{15}$ Hz. The techniques available, each probing a fraction of the frequency spectrum, hence give different values and information.

THz-TDS measures complex permittivity at frequencies between 0.3–5 THz. It is a pulsed technique, with the pulse duration being about 1 ps and repetition rate about 80 MHz. Therefore, it observes dielectric response at THz frequencies on timescales of a few ps. EIS measures steady-state impedance at a range of frequences, typically up to a few MHz, with the possibility of a few GHz. At these frequencies, dielectric response differs significantly from its values at THz (Fig. 1a); and moreover, complex permittivity cannot be obtained straightforwardly from impedance, requiring complex equivalent circuit models. SE measures the changes in amplitude and phase at specific photon energies in the visible and near-infrared at differing angles of incidence, from which constants such as refractive index and absorption coefficient are extracted through an optical model, thus rendering it an indirect method of complex permittivity characterisation. At these frequencies, using light in the UV-vis-NIR, dielectric response differs significantly from its values at THz, especially so in materials possessing a Reststrahlen band.[17]

Given the novelty of the terahertz dielectric property measurements for carbon nitride polymorphs reported herein,

we can now place our results in the context of current literature available on these materials, measured with standard techniques such as EIS and Spectroscopic Ellipsometry (SE). These probe the low-mid frequency (10^{-3} to 10^{6} Hz), and very high frequency range accessible by UV-NIR ellipsometry (10^{14} to 10^{16} Hz), respectively and provide the DC and ultrafast ε' values often referred to as extremes, since other data is missing. The trends in real permittivity ε', summarized in Fig. 5, illustrate that the THz measurements indeed show intermediate values following the expected trend with frequency: EIS estimated ε' to have values at ~15 and 7 at 10^{-3}-10^{5} Hz for K-PHI and g-C_3N_4 in ambient conditions, respectively.[25,61] Both drop significantly to ~7 and ~5 at 1.5 THz (−53% and −29%). In the 10^{14}–10^{15} Hz SE-regime (also ambient conditions), melon stays constant (~5),[62] while K-PHI further decreases to ~3, [63] which corresponds to its dry value at ~2 THz.

The parallel trend between EIS and THz-TDS, with K-PHI retaining its higher dielectric response compared with melon in ambient conditions up to the THz regime, indicates that both EIS and THz-TDS are suitable for a relative comparison of materials in their real permittivity response, including ambient & humidity effects. SE may capture contributions from electronic polarisation at ultrafast timescales (several fs), as these optical excitations are too fast for atomic or molecular rearrangements in either water or CN_x materials. Consequently, we observe a similarity between THz permittivity in the dry state, and the one extracted from SE in both melon and K-PHI.

This shows that drawing conclusions about intermediate and especially THz processes from EIS & SE measurements alone may be insufficient, and that separate THz analysis is crucial for capturing different phenomena on its timescales. This THz-characterization is even more relevant if materials are involved where illumination generates carriers that are key to function on the picosecond timescale. The drop from ε'_{DC} (static dielectric response) or EIS to ε'_{THz} is hard to extrapolate, and may be different even for similar materials, as shown here for g-C_3N_4 *vs.* PHI. While SE may enable estimation of the THz permittivity response in dry conditions, the result may be strongly modified in reality – by ambient effects, ionic or other phenomena in the THz regime, and on slower times. As such, the real permittivity at the low or high frequency limit provides insufficient information on the functionality of materials used for energy conversion.

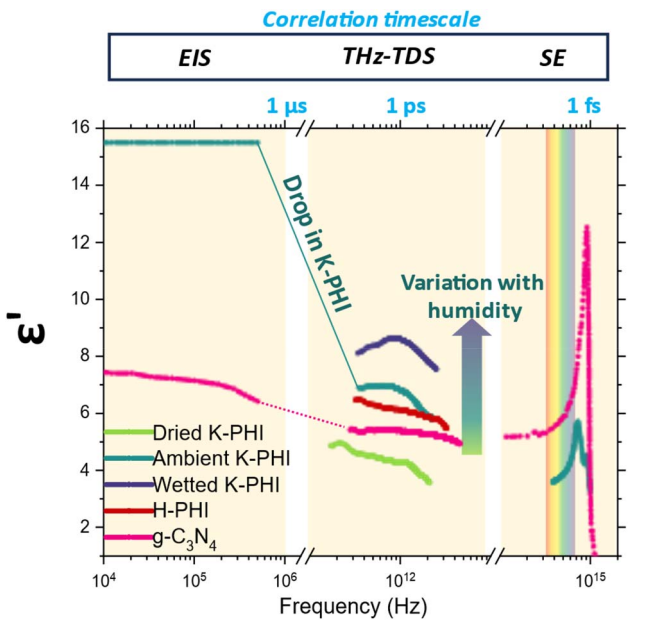

Fig. 5 Real permittivity comparison over the frequency spectrum for melon and K-PHI, with data extracted from Electrochemical Impedance Spectroscopy (EIS), THz (data from Fig. 2) and Spectroscopic Ellipsometry (SE) (literature values reproduced under CC by 4.0 license),[47,62,63] confirming the predicted dispersive trends in real permittivity (Fig. 1a).

Water and wetting groups

The presence of water, or its inclusion by wetting groups with high static real permittivity ε'_{DC} (*e.g.* ethylene glycol),[15,64] was discussed earlier in relation to its ability to boost photocatalytic efficiency of polymers *e.g.* through enhanced permittivity (measured by EIS).[65–67] While water has a high dielectric response in the low frequency regime, this is not the case in the THz regime. Hence, it can increase the response of materials with lower ε' values than itself (ε' ~2.77 for ambient PEG-8000 *vs.* 4.1 for water at 1.5 THz) from a linear combination of water + material, especially in wetting materials, but this effect may be smaller than expected (2–5% changes observed for poly(ethylene glycol)). However, it was not previously clear *a priori* that ε' can be increased for materials that have larger ε' values than water, like CN_x,[27] where we now revealed synergistic effects beyond those expected from a linear combination of the material and water alone. Hence, when charge stabilizing effects through wetting groups are observed on in ultrafast (fs-ns) spectroscopy measurements (and not only on sub-µs time scales corresponding to EIS analysis) in solar cell or photocatalyst materials, they may likely be linked also to modified THz properties, which can in future be studied separately by THz-TDS – giving a better approximation to applications also involving water, or other environments in principle.

Solar energy conversion

Despite the importance of understanding (modified) permittivity on THz timescales *vs.* mHz–MHz timescales (EIS) or SE, it remains an open question as to which timescale is most relevant for enhancing light-energy conversion function. The result likely depends on the application scenario and on the bottleneck in the process, *i.e.* on morphological factors (*e.g.* particle size, grain boundary density and their effects), on the function and density of intrinsic traps, and on transport properties – *i.e.* the ability to make use of light generated charges after collecting them.[4,60,68,69] While the fast timescales are crucial for exciton dissociation and charge carrier generation, they don't have to be limiting (see hybrid perovskites, or $SrTiO_3$ enabling 100% photocatalytic quantum efficiency as perfectly engineered cases[70]), and slower (µs-s) times scales may also be highly

relevant for photocatalytic function, since surface catalytic processes are often slow, requiring charge stabilization.[71,72]

A common method to increase the low frequency permittivity is to add functional groups like ethylene glycol with high ε' values at low frequences to polymers with intrinsically lower ε' values.[15,64] These functionalizations are reported to increase the conversion efficiency of sunlight to hydrogen in photocatalysis due to various effects occurring on different timescales including the ns-regime,[15] but their influence is most clear in the lifetime of charges extending to the μs-s range (corresponding to EIS frequencies, *i.e.* 1 Hz–1 MHz) due to enhanced polarizability of the material. However, less is known about the functional groups' direct influence on exciton dissociation to charges, which still is a major bottleneck in photocatalysis with organic materials and related solar energy conversion technologies. THz-TDS complex permittivity analysis, carried out herein, can in principle provide insights on the origin of photophysical interaction effects expected in the sub-ps timescale, and thus directly support description of exciton stability (lifetime) and charge generation. At present, such phenomena are typically measured using fs-ns TAS, which is unable to provide direct photophysical material properties like ε' and can be difficult to interpret due to the high photon fluxes used in the excitation pulse experiments. Further, for the purposes of material modelling and property prediction, knowledge of the complex permittivity at given timescales is key to correctly elucidate corresponding properties and behaviour of functional interest. This is especially key in the context of Artificial Intelligence (AI) and Machine Learning, *e.g.* if targeting improved synthetic (bottom-up) design, which is particularly promising with organic materials. THz measurements easily provide such valuable insights, without complex models or assumptions being required.

Potential for light-driven ionics

Enhanced THz ε' relative to melon is herein clearly visible. Further, the presence of aqueous alkali metal ions contributes to THz polarization of the material, and to differently pronounced relaxation mechanisms on the ps-scale. Since permittivity increases because of higher polarizability, the enhanced ε' in K-PHI indirectly show that also light-driven generation of charges may in turn affect structural hydrated K^+ ions on picosecond timescales. As such, these insights also possibly point to efficient optoionic or photocharging interactions, where ions stabilize charge carriers on ultrafast time scales.[73,74] In K-PHI, such optoionic stabilization (being mediated by water) occurs on the fs-ps regime – where light generated charge carriers can interact with internal or external (solvated) ions, modifying the material's stoichiometry and with that, photophysical properties. The presence of these alkali metal ions is key to enable photocharging, *i.e.* the intrinsic combination of light absorption (solar cell function) and charge storage (battery function) properties. Besides photobatteries, this can be used for effects like dark photocatalysis, for powering microparticles, and for sensing etc.[20,41–43,63,75] An ionically enhanced permittivity on the THz timescale is expected to be beneficial for generating and/or stabilizing photogenerated charges quickly and efficiently. We therefore suggest that the overall strength optoionic effects and the efficiency of photocharging materials and light-driven ionotronic devices may benefit from enhanced THz permittivities.[76–78]

Summary & outlook

This work presents THz-TDS is a powerful, non-destructive, and non-contact tool for directly characterizing the complex permittivity $\boldsymbol{\varepsilon}$ of organic semiconductors. It provides valuable insights into their dielectric response and related properties (*e.g.* THz conductivity). This characterization on the sub-ps timescale closes the "THz gap" (Fig. 1a) resulting from limitations to EIS (mHz to 10^6 Hz), microwave dielectric measurements (GHz timescales) and SE (10^{14} to 10^{16} Hz). Different polarization processes occur on respective timescales, resulting in timescale-dependent trends and environmental effects that are difficult to extrapolate based on measurements made on non-corresponding timescales. The THz regime encompasses processes on time scales involving exciton generation and separation as well as fast charge relaxation effects. Hence, the characterization of complex permittivity by THz-TDS can provide a broader understanding of functional materials used for light conversion applications, including photovoltaics, photodetectors and photocatalysts, and enable more accurate modelling from knowledge of (photo)physical properties. For example, Fig. 4 compares the $\varepsilon'_{1.5\mathrm{THz}}$ of materials used for such applications, pointing out that inorganics used for solar energy conversion are not necessarily very high dielectrics in the THz regime, and that CN_x has comparable dielectric properties on this timescale. Hence, their photophysical properties for solar energy conversion are probably less limited by exciton dissociation, compared to traditionally used semiconducting polymers.

This study further highlights the importance of structurally adsorbed water being able to synergistically enhance the complex permittivity in the THz-regime. Here, a more straightforward and unambiguous characterization of contributions from the backbone, water and ions become possible when comparing to probing techniques like EIS and SE. Hence, care must be taken when comparing measurements acquired in different conditions, and when materials are employed in humid environments, it is important bear in mind that the properties of dry materials may be significantly different from those occurring in real application scenarios (such as photocatalytic reactions in water or other electrolytes). This is also relevant for modelling purposes, which often neglect environmental factors, or might use dielectric properties as input parameters, which cannot be generalized from other frequency domains, and would neglect synergistic effects seen here in the THz regime.

The use of THz-TDS, being increasingly available, is hence highly recommended for characterization of functional materials used in solar energy conversion, or with crucial function in the (sub–)ps regime. In particular, the surprising findings of structural water or hydrated ions apparently contributing to the

real dielectric permittivity response even on ps timescales (promoted *via* ambient humidity, increasing the response beyond the material's backbone alone) sheds further light on material analysis and selection for future ionotronic materials operating on THz timescales – for which K-PHI or other porous framework materials containing ions, like COFs, MOFs or porous (ionic) polymers may be good candidates. THz-TDS also enables direct extraction of their conductivity σ_{THz} without further approximations. Further, direct light-driven ionic effects (optoionics) may potentially be characterized more directly by this technique in the future. The ability of soft ionic materials to exhibit strongly enhanced permittivities in the presence of water may help to combat the often-limiting strong exciton recombination seen in apparently low dielectric materials – and often targeted by wetting – although without knowledge of its fs-ps time scale influence. THz-TDS may hence be a key component for addressing fundamental challenges of organic semiconductors and their applicability for solar energy conversion and thus be an enabler in the transition to a more sustainable energy economy and the development of related materials infrastructure.

Author contributions

J. D., M. N. and F. P. designed and supervised the project. F. P. and P. A. synthesized and prepared the CN_x materials. D. S. and S. S. performed and analysed density measurements, P. A the XRD measurements. R. J. and F. P. prepared CN_x pellets for characterisation. R. J. and F. P. measured contact angles. R. J. measured and analysed the THz data, with assistance and supervision of M.N. F. P. and S. H. prepared, performed, and analysed fs-ns TAS measurements. F. P. and R. J. wrote the manuscript draft. All authors incl. A. K. contributed to manuscript revisions and discussions.

Conflicts of interest

There are no conflicts of interest to declare.

Data availability

The data reported in this study will be shared on the research repository zenodo following acceptance. See DOI: 10.5281/zenodo.18551232.

Supplementary information (SI) is available. See DOI: https://doi.org/10.1039/d5el00170f.

Acknowledgements

The authors acknowledge Dr Carolina Pulignani and Prof. Erwin Reisner (Dep. Of Chemistry, University of Cambridge) for providing carbon nitrides for this study, Dr Nuria Tapia-Ruiz and Sarah McKinney for use of their labs and assistance in pellet preparation, and Dr Andrew Gregory for use of his in-house NPL THz-TDS software for thickness optimisation. Dr Julia Kröger (EnBW) and Prof. Ji-Seon Kim (Imperial) are acknowledged for fruitful discussions. F. P. and J. D. acknowledge funding from UKRI (grant reference EP/X027449/1) and EPSRC (grant reference EP/Z536258/1). F. P. further acknowledges funding from The Royal Society (URF\R1\251843), and J. D. from EPSRC (grant reference EP/T028513/1). P. A. thanks the Science and Solutions for a Changing Planet DTP (NE/S007415/1), hosted at the Grantham Institute for Climate Change and the Environment for funding this research. A. K. thanks the EPSRC for a Programme Grant (EP/W017075/1). Work at the National Physical Laboratory was supported by the UK Government's Department for Science, Innovation and Technology (DSIT) through the UK's National Measurement System programs.

References

1 H. Naito, *Organic semiconductors for optoelectronics*, Wiley, 2021.
2 M. T. Sajjad, A. Ruseckas and I. D. W. Samuel, *Matter*, 2020, **3**, 341.
3 H. Bronstein, C. B. Nielsen, B. C. Schroeder and I. McCulloch, *Nat. Rev. Chem.*, 2020, **4**, 66.
4 T. Banerjee, F. Podjaski, J. Kröger, B. P. Biswal and B. V. Lotsch, *Nat. Rev.*, 2021, **6**, 168.
5 O. V Mikhnenko, P. W. M. Blom and T.-Q. Nguyen, *Energy Environ. Sci.*, 2015, **8**, 1867.
6 Y.-X. Li and W. Choi, *Chem Catal.*, 2022, **2**, 1517.
7 Q. Zhou, Y. Guo and Y. Zhu, *Nat. Catal.*, 2023, **6**, 574.
8 J. W. Schultz, *Focused beam methods: measuring microwave materials in free space*, CreateSpace Independent Publishing Platform, Atlanta GA, USA, 2012.
9 R. A. Alahnomi, Z. Zakaria, Z. M. Yussof, A. A. Althuwayb, A. Alhegazi, H. Alsariera and N. A. Rahman, *Sensors*, 2021, **21**, 2267.
10 J. T. Kindt and C. A. Schmuttenmaer, *J. Phys. Chem.*, 1996, **100**, 10373.
11 T. Mosavirik, M. Soleimani, V. Nayyeri, S. Hossein Mirjahanmardi, G. Student Member, M. Soleimani, S. Member and O. M. Ramahi, *IEEE Trans. Instrum. Meas.*, 2021, **70**, 1.
12 A. Armin, D. M. Stoltzfus, J. E. Donaghey, A. J. Clulow, R. C. R. Nagiri, P. L. Burn, I. R. Gentle and P. Meredith, *J. Mater. Chem. C*, 2017, **5**, 3736.
13 N. Mallo, S. McAnally, R. Chu, M. Babazadeh, H. Jin, P. L. Burn, I. R. Gentle and P. E. Shaw, *J. Mater. Chem. C*, 2023, **11**, 14382.
14 Z. Fu, X. Zhang, H. Zhang, Y. Li, H. Zhou and Y. Zhang, *Chin. J. Chem.*, 2021, **39**, 381.
15 J. Kosco, S. Gonzalez-Carrero, C. T. Howells, W. Zhang, M. Moser, R. Sheelamanthula, L. Zhao, B. Willner, T. C. Hidalgo and H. Faber, *Adv. Mater.*, 2022, **34**, 2105007.
16 W. J. Ellison, *J. Phys. Chem. Ref. Data*, 2007, **36**, 1.
17 M. Koch, D. M. Mittleman, J. Ornik and E. Castro-Camus, *Nat. Rev. Methods Primers*, 2023, **3**, 48.
18 J. Neu and C. A. Schmuttenmaer, *J. Appl. Phys.*, 2018, **124**(23), 124.
19 X. Huang, X. Wang, Y. Zou, M. An and Y. Wang, *Small*, 2024, **20**, 2400874.

20 O. Savateev, M. Antonietti and X. Wang, *Carbon nitrides : structure, properties and applications in science and technology*, De Gruyter, Berlin, 2023.
21 B. V. Lotsch, M. Döblinger, J. Sehnert, L. Seyfarth, J. Senker, O. Oeckler and W. Schnick, *Chem. Eur J.*, 2007, **13**, 4969.
22 O. Ostroverkhova, *Chem. Rev.*, 2016, **116**, 13279.
23 A. Savateev, S. Pronkin, M. G. Willinger, M. Antonietti and D. Dontsova, *Chem.–Asian J.*, 2017, **12**, 1517.
24 H. Schlomberg, J. Kröger, G. Savasci, M. W. Terban, S. Bette, I. Moudrakovski, V. Duppel, F. Podjaski, R. Siegel, J. Senker, R. E. Dinnebier, C. Ochsenfeld and B. V. Lotsch, *Chem. Mater.*, 2019, **31**, 7478.
25 J. Kröger, F. Podjaski, G. Savasci, I. Moudrakovski, A. Jiménez-Solano, M. W. Terban, S. Bette, V. Duppel, M. Joos, A. Senocrate, R. Dinnebier, C. Ochsenfeld and B. V. Lotsch, *Adv. Mater.*, 2022, **34**, e2107061.
26 J. F. Federici, *J. Infrared Millim. Terahertz Waves*, 2012, **33**, 97.
27 Z. Zang, Z. Li, X. Lu, J. Liang, J. Wang, H.-L. Cui and S. Yan, *Comput. Electron. Agric.*, 2021, **191**, 106515.
28 L. Quancheng, L. Xiaoxia, D. Hu, S. Jingxin, G. Deyun, L. Lichuan, Z. Yuzhe and S. Liping, *Opt. Eng.*, 2020, **59**, 84102.
29 X. Chen, D. Cao, H. Chen, X. He, G. Fang and X. Chen, *Photonics Res.*, 2025, **14**, 230.
30 G.-H. Oh, H.-S. Kim, D.-W. Park and H.-S. Kim, *Opt Laser. Eng.*, 2020, **128**, 106036.
31 W. Si, Q. Liao, W. Hou, L. Chen, X. Li, Z. Zhang, M. Sun, Y. Song and L. Qin, *Coatings*, 2022, **12**, 766.
32 D. J. Martin, K. Qiu, S. A. Shevlin, A. D. Handoko, X. Chen, Z. Guo and J. Tang, *Angew. Chem.*, 2014, **126**, 9394.
33 X. Wang, Y. Ren, Y. Li and G. Zhang, *Chemosphere*, 2022, **287**, 132098.
34 G. J. Hutchings, P. R. Davies, S. Pattisson, T. E. Davies, D. J. Morgan and M. W. Dlamini, *Catal. Commun.*, 2022, **169**, 106480.
35 M. Naftaly, I. Tikhomirov, P. Hou and D. Markl, *Sensors*, 2020, **20**, 3120.
36 P. U. Jepsen and B. M. Fischer, *Opt. Lett.*, 2005, **30**, 29.
37 A. Bergner, U. Heugen, E. Bründermann, G. Schwaab, M. Havenith, D. R. Chamberlin and E. E. Haller, *Rev. Sci. Instrum.*, 2005, **76**, 63110.
38 A. M. Ulatowski, L. M. Herz and M. B. Johnston, *J. Infrared Millim. Terahertz Waves*, 2020, **41**, 1431.
39 D. Burmeister, A. Eljarrat, M. Guerrini, E. Röck, J. Plaickner, C. T. Koch, N. Banerji, C. Cocchi, E. List-Kratochvil and M. J. Bojdys, *Chem. Sci.*, 2023, **14**, 6269.
40 A. Puthukkudi, S. Nath, P. Shee, A. Dutta, C. V Rajput, S. Bommakanti, J. Mohapatra, M. Samal, S. Anwar and S. Pal, *Adv. Mater.*, 2024, **36**, 2312960.
41 H. Kasap, C. A. Caputo, B. C. M. Martindale, R. Godin, V.-H. Lau, B. V. Lotsch, J. R. Durrant and E. Reisner, *J. Am. Chem. Soc.*, 2016, **138**(29), 9183–9192.
42 V. W. Lau, D. Klose, H. Kasap, F. Podjaski, M. Pignié, E. Reisner, G. Jeschke and B. V. Lotsch, *Angew. Chem.*, 2017, **129**, 525.
43 F. Podjaski, J. Kröger and B. V. Lotsch, *Adv. Mater.*, 2018, **30**, 1705477.
44 W. Yang, R. Godin, H. Kasap, B. Moss, Y. Dong, S. A. J. Hillman, L. Steier, E. Reisner and J. R. Durrant, *J. Am. Chem. Soc.*, 2019, **141**(28), 11219–11229.
45 A. Gouder, A. Jiménez-Solano, N. M. Vargas-Barbosa, F. Podjaski and B. V. Lotsch, *Mater. Horiz.*, 2022, **9**, 1866.
46 J. Zhang, T. Bai, W. Liu, M. Li, Q. Zang, C. Ye, J. Z. Sun, Y. Shi, J. Ling and A. Qin, *Nat. Commun.*, 2023, **14**, 3524.
47 P. Giusto, D. Cruz, T. Heil, H. Arazoe, P. Lova, T. Aida, D. Comoretto, M. Patrini and M. Antonietti, *Adv. Mater.*, 2020, **32**, e1908140.
48 S. R. Konda, Y. Lin, R. A. Rajan, W. Yu and W. Li, *Materials*, 2023, **16**, 610.
49 I. Maeng, S. Chen, S. Lee, S. Wang, Y.-K. Kwon and M.-C. Jung, *Mater. Today Phys.*, 2023, **30**, 100960.
50 J. Calvo-de La Rosa, A. Locquet, D. Bouscaud, S. Berveiller and D. S. Citrin, *IEEE Trans. Terahertz Sci. Technol.*, 2021, **11**, 402.
51 D. Grischkowsky, S. Keiding, M. van Exter and C. Fattinger, *J. Opt. Soc. Am. B*, 1990, **7**, 2006.
52 A. Deneuville, D. Tanner and P. H. Holloway, *Phys. Rev. B*, 1991, **43**, 6544.
53 C. M. Randall and R. D. Rawcliffe, *Appl. Opt.*, 1968, **7**, 213.
54 M. T. Hibberd, V. Frey, B. F. Spencer, P. W. Mitchell, P. Dawson, M. J. Kappers, R. A. Oliver, C. J. Humphreys and D. M. Graham, *Solid State Commun.*, 2016, **247**, 68.
55 I. D. Vugmeyster, J. F. Whitaker and R. Merlin, *Appl. Phys. Lett.*, 2012, **101**, 181101.
56 M. Mumtaz, M. A. Mahmood, S. D. Khan, M. A. Zia, M. Ahmed and I. Ahmad, *Opt. Mater.*, 2019, **96**, 109357.
57 G. B. Netto and J. D. P. Siqueira, F. C. Da Cruz, in *2023 Int. Conf. Opt. MEMS Nanophotonics Sbfot. Int. Opt. Photonics Conf. (Sbfot. IOPC)*, IEEE, 2023, pp. 1–2.
58 A. K. Azad, J. Han and W. Zhang, *Appl. Phys. Lett.*, 2006, **88**, 021103.
59 G. Zhang, G. Li, Z. Lan, L. Lin, A. Savateev, T. Heil, S. Zafeiratos, X. Wang and M. Antonietti, *Angew. Chem.*, 2017, **129**, 13630.
60 J. Kröger, A. Jiménez-Solano, G. Savasci, V. W. h. Lau, V. Duppel, I. Moudrakovski, K. Küster, T. Scholz, A. Gouder, M. Schreiber, F. Podjaski, C. Ochsenfeld and B. V. Lotsch, *Adv. Funct. Mater.*, 2021, **31**, 2102468.
61 P. C. Patra and Y. N. Mohapatra, *Appl. Phys. Lett.*, 2021, **118**, 103501.
62 T. Berlind, A. Furlan, Z. Czigany, J. Neidhardt, L. Hultman and H. Arwin, *Thin Solid Films*, 2009, **517**, 6652.
63 A. Gouder, L. Yao, Y. Wang, F. Podjaski, K. S. Rabinovich, A. Jiménez-Solano and B. V. Lotsch, *Adv. Energy Mater.*, 2023, **13**, 2300245.
64 D. J. Woods, S. A. J. Hillman, D. Pearce, L. Wilbraham, L. Q. Flagg, W. Duffy, I. McCulloch, J. R. Durrant, A. A. Y. Guilbert, M. A. Zwijnenburg, R. S. Sprick, J. Nelson and A. I. Cooper, *Energy Environ. Sci.*, 2020, **13**, 1843.
65 M. Sachs, R. S. Sprick, D. Pearce, S. A. J. Hillman, A. Monti, A. A. Y. Guilbert, N. J. Brownbill, S. Dimitrov, X. Shi, F. Blanc, M. A. Zwijnenburg, J. Nelson, J. R. Durrant and A. I. Cooper, *Nat. Commun.*, 2018, **9**, 4911.

66 J. Choi, W. Jung, S. Gonzalez-Carrero, J. R. Durrant, H. Cha and T. Park, *Energy Environ. Sci.*, 2024, **17**(21), 7999–8018.
67 M. J. Zouaoui, B. Nait-Ali, N. Glandut and D. S. Smith, *J. Eur. Ceram. Soc.*, 2016, **36**, 163.
68 Y. Wang, A. Vogel, M. Sachs, R. S. Sprick, L. Wilbraham, S. J. A. Moniz, R. Godin, M. A. Zwijnenburg, J. R. Durrant, A. I. Cooper and J. Tang, *Nat. Energy*, 2019, **4**, 746.
69 S. Corby, R. R. Rao, L. Steier and J. R. Durrant, *Nat. Rev. Mater.*, 2021, **6**, 1136.
70 T. Takata, J. Jiang, Y. Sakata, M. Nakabayashi, N. Shibata, V. Nandal, K. Seki, T. Hisatomi and K. Domen, *Nature*, 2020, **581**, 411.
71 R. Godin and J. Durrant, *Chem. Soc. Rev.*, 2021, **50**, 13372.
72 J. Kosco, S. Gonzalez-Carrero, C. T. Howells, T. Fei, Y. Dong, R. Sougrat, G. T. Harrison, Y. Firdaus, R. Sheelamanthula and B. Purushothaman, *Nat. Energy*, 2022, **7**, 340.
73 A. Senocrate, E. Kotomin and J. Maier, *Helv. Chim. Acta*, 2020, **103**, e2000073.
74 F. Podjaski and B. V. Lotsch, *Adv. Energy Mater.*, 2021, **11**, 2003049.
75 V. Sridhar, F. Podjaski, Y. Alapan, J. Kröger, L. Grunenberg, V. Kishore, B. V. Lotsch and M. Sitti, *Sci. Robot.*, 2024, **7**, eabm1421.
76 A. Rogolino and O. Savateev, *Adv. Funct. Mater.*, 2023, **33**, 2305028.
77 C. Wan, K. Xiao, A. Angelin, M. Antonietti and X. Chen, *Adv. Intell. Syst.*, 2019, **1**, 1900073.
78 V. Druet, D. Ohayon, C. E. Petoukhoff, Y. Zhong, N. Alshehri, A. Koklu, P. D. Nayak, L. Salvigni, L. Almulla and J. Surgailis, *Nat. Commun.*, 2023, **14**, 5481.